Coarse-graining the electron distribution in turbulence simulations of tokamak plasmas[a)]

Yang Chen,[1,b)] Scott E. Parker,[1] Gregory Rewoldt,[2] Seung-Hoe Ku,[3] Gun-Young Park,[3] and C-S Chang[3]
[1]*University of Colorado at Boulder, Boulder, Colorado 80309, USA*
[2]*Princeton Plasma Physics Laboratory, Princeton, New Jersey 08543, USA*
[3]*New York University, New York, New York 10003, USA*

(Received 16 November 2007; accepted 22 January 2008; published online 12 March 2008)

The coarse-graining procedure (CGP) [Y. Chen and S. E. Parker, Phys. Plasmas **14**, 082301 (2007)] is implemented in the GEM code for electrons. While CGP introduces numerical dissipation in the particle-in-cell simulations, it is shown that CGP preserves physical dissipation effects such as the electron-ion collisional effects on the particle flux in ion-temperature-gradient driven turbulence. Kinetic simulation of an edge plasma is presented, which demonstrates the essential stabilizing effect of shear flow and the destabilizing effect of magnetic field perturbation in such a plasma.
 [DOI: 10.1063/1.2884040]

I. INTRODUCTION

It is now well known that the mean square of particle weights in δf particle-in-cell (PIC) simulations of turbulent transport continues to grow, although the turbulent fluxes can apparently reach a steady state. The reason is twofold. In a collisionless simulation, the entropy ($\int \delta f^2/f_0 d\mathbf{x}d\mathbf{v}$) necessarily evolves when there is a nonzero turbulent flux. Particle collisions, when implemented as a random scattering of particle velocities, cause the particle weights at a given phase-space location to broaden in time. Both effects increase the mean-square value of the particle weights. Since the discrete particle noise in PIC simulation is proportional to the particle weights, it is desirable to suppress or reduce the long-term particle weight growth in PIC simulations. In a previous study,[1] we presented a coarse-graining procedure (CGP) for this purpose. In CGP, the particle distribution is periodically constructed on a five-dimensional (5D) phase-space grid by depositing the particle weights on the grids. This grid-based distribution function is then interpolated at the particle location to obtain a new particle weight. The procedure is demonstrated to effectively suppress the ion particle weight growth in a flux-tube simulation of ion-temperature-gradient (ITG) turbulence with adiabatic electrons. It is shown that in the steady state, the increase to the particle weights due to nonzero ion heat flux is balanced by CGP, making it possible for the mean square of weights to saturate. Because the kinetic distribution is smoothed over a small but finite phase-space volume, CGP effectively introduces numerical dissipation in the kinetic equation. An upper bound for the equivalent dissipation rate due to CGP was derived. However, the actual dissipation rate is unknown, since it depends on how frequently a particle weight is reset, hence on how many particles are used in the simulation. In a situation in which the physical collisions are important, the dissipation rate due to CGP must not exceed the physical collision rate. This raises the question of whether a window of the CGP frequency exists such that the long-term particle weight growth can be effectively reduced, while the physical collision effect is not distorted by the numerical dissipation.

In this paper, we apply CGP to the electrons. We use the particle pinch phenomenon of ITG instabilities to compare the dissipative effect of CGP with physical collisional effects. Particle flux in ITG instabilities with kinetic electrons is frequently observed to be directed inward. This particle pinch is believed to be due to the nonadiabatic effects of passing electrons in a mode elongated along the magnetic field.[2] Both finite-β effects and electron-ion (e-i) collisions can cause the particle flux to be directed outward. The coarse-graining procedure also changes the direction and magnitude of the particle flux. The ratio of the quasilinear particle flux to the ion heat flux depends sensitively on both the e-i collision rate and CGP frequency. This provides a way to quantify the numerical dissipation of CGP. It is found that for typical CGP parameters, the equivalent dissipation rate is very small, i.e., CGP preserves linear collisional effects. Using an ITG case based on the Cyclone Base Case Parameters,[3] we also show that for typical CGP frequency the nonlinear effect of e-i collisions on the particle flux is also preserved.

The simulations presented here are done with the (global) GEM code,[4] which uses the Miller magnetohydrodynamics (MHD) equilibrium.[5,6] The GEM code has been interfaced with the TRANSP code,[7] along with the NCLASS[8] and JSOLVER[9] codes, for modeling the National Spherical Torus Experiment (NSTX) and DIII-D experiments. Four particle species are currently included: the main ion species, an impurity species, a hot beam ion species, and electrons. Flux surface shape profiles for elongation, triangularity, and the Shafronov shift, the density and temperature profiles for each species, and the $\mathbf{E}\times\mathbf{B}$ and parallel flow profiles are all obtained from TRANSP analysis along with NCLASS and JSOLVER. Simulations frequently indicate that the anomalous transport levels sensitively depend on the experimental pro-

[a)]Paper BI2 5, Bull. Am. Phys. Soc. **52**, 24 (2007).
[b)]Invited speaker.

files, in particular the $\mathbf{E}\times\mathbf{B}$ flow profiles. We will report further on the results of applying GEM to NSTX and DIII-D plasmas in the future, but in this paper we use an edge pedestal plasma with strong profile variations to show the strong dependence of transport on flow profiles. The pedestal structure is output from XGC0 guiding-center particle simulations.[10] This is partly motivated by previous studies of trapped electron mode (TEM) turbulence[11] using flux-tube simulations. It was found in flux-tube simulations that when the density gradient increases from typical core values but is still well below that of pedestal plasmas ($R/L_n \sim 100$), flux-tube simulations do not saturate. In those flux-tube simulations, magnetic perturbation was not considered, and there were no profile variations and no equilibrium plasma flows, which are obvious stabilizing mechanisms in plasma regions with steep density gradients. The simulations presented here indicate that all these effects (plasma flows, profile variations, and magnetic perturbations) are important for edge plasmas.

II. IMPLEMENTATION OF THE COARSE-GRAINING PROCEDURE IN GEM

Here the implementation of CGP in GEM is summarized. The implementation of CGP in a global code differs from that in a flux-tube code mainly in the choice of the energy-like variable, due to the radial dependence of the temperature. In general, both the equilibrium density and temperature are allowed to vary arbitrarily across the radial domain. Marker particles, on the other hand, are loaded to have constant density in radius, in order to have a balanced particle loading.[4] Marker particles are still loaded according to the equilibrium temperature profile. In principle this is not necessary: particles can be loaded with a constant temperature radially. The temperature can be chosen to be the maximum temperature in the simulation domain. As long as the particle number is sufficiently large, so that there are sufficient particles with energies within a few times the temperature at each radial location, the δf method is valid. Loading particles this way has the advantage of avoiding marker profile relaxation due to turbulent transport. (Real profile relaxation still occurs, and is represented by δf through the particle weights. This will be discussed further in Sec. IV.) However, this is numerically inefficient, since at radial locations with much smaller temperature a large number of markers have energies many times larger than the local temperature, with their weights essentially zero.

For a marker population distributed according to the physical temperature $T(r)$, the energy variable for CGP is defined to be $E=mv^2/2T(r)$. The other velocity variable used for CGP is the pitch angle variable $\lambda=v_\parallel/v$. At each spatial grid (x_i,y_j,z_k), the velocity space is divided into $N_E N_\lambda$ grids, equally spaced in E and λ. CGP consists of two passes of traversing through the particle array. During the first traversal, the distribution function is constructed on the 5D phase-space grids, by depositing the particle weights to nearby grids. Both the nearest-grid-point (NGP) algorithm and linear interpolation (LI) can be used for the deposition, and the choice can vary among the phase-space dimensions. During the second traversal of the particle array, the above constructed distribution is used to reset the particle weight at the particle position, using the same interpolation scheme. This is done every N_s steps. At each CGP, the actual particle weight is reset according to the lag-average formula,

$$w'' = (1-\delta)w + \delta w', \tag{1}$$

with $\delta \ll 1$. Here w' is the weight obtained from the nearby grid points using interpolation.

III. COARSE-GRAINING AND COLLISIONAL EFFECT

Since coarse-graining introduces numerical dissipation into the simulation, it is important to ensure that the physical collisional effect is not obscured by CGP. Previously CGP was studied using ITG turbulence as a test problem. In Ref. 1, it is shown that simulations with $N_s=10$, $\delta=0.1$ yield the same turbulent ion heat diffusivity as the simulation with no CGP. In fact, we found that even if CGP is done every time step with $\delta=0.5$, the turbulent diffusivity is not significantly changed. The ITG turbulence with the adiabatic electron assumption is surprisingly tolerant of aggressive coarse-graining, and is not suitable for studying the effect of CGP in the presence of collisions.

Electron-ion collisions are stabilizing on the ITG instabilities. However, a collision rate much larger than the realistic value has to be used to observe this stabilizing effect in benchmarking studies.[12] We therefore turn to another collisional effect on the ITG instabilities, namely the collisional effect on the quasilinear particle diffusivity of ITG modes. In both flux-tube and global simulations of ITG instabilities with kinetic electrons, the particle flux is frequently observed to be directed inward. This pinch is sensitive to the electron-ion collision rate and CGP frequency, and can be used to compare numerical dissipation with physical dissipation. We define the quasilinear particle flux

$$\Gamma_p = \frac{n_0}{N}\sum_j w_j v_{\mathrm{Ex}} \tag{2}$$

and the quasilinear energy flux

$$\Gamma_e = \frac{n_0}{N}\sum_j w_j \epsilon_j v_{\mathrm{Ex}}, \tag{3}$$

where N is the number of particles. In a linear simulation, both Γ_p and Γ_e grow at a growth rate twice the mode growth rate, but the ratio $\Gamma_p T_0/\Gamma_e$ is a dimensionless constant that is determined by the unstable eigenmode. This ratio can be used as an indicator of how much dissipation is present.

Consider a hydrogen plasma with $R/a=3$; at $r_0/a=0.5$, the local density and temperature gradients are given by $R_0/L_T=9$ and $R_0/L_n=3$, the magnetic shear $s_0=r_0q'/q_0=1$ and $q_0=2$. Figure 1 shows the effects of coarse-graining on the ratio $\Gamma_p T_0/\Gamma_e$ for the $n=18$ mode. Coarse-graining is done with $N_s=10$, i.e., every 10 time steps, with δ varied from 0.01 to 0.5. The e-i collision rate is set to zero when coarse-graining is done. Another set of linear runs is carried out, with $\delta=0$ (no CGP) but nonzero e-i collision rate. The results are also plotted in Fig. 1. The maximal e-i collision rate, $\nu_{\mathrm{ei}}/\Omega_{\mathrm{ci}}=10^{-4}$, is meant to be representative of experi-

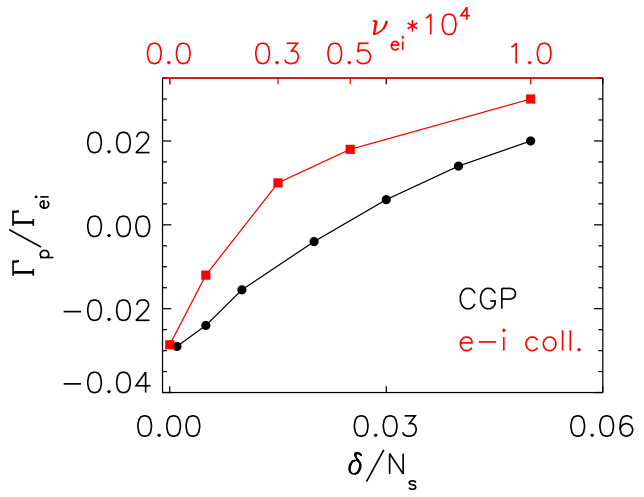

FIG. 1. (Color online) Effects of dissipation on particle flux in linear simulations. Black points are results of coarse-graining, red/light gray points are results of e-i collisions.

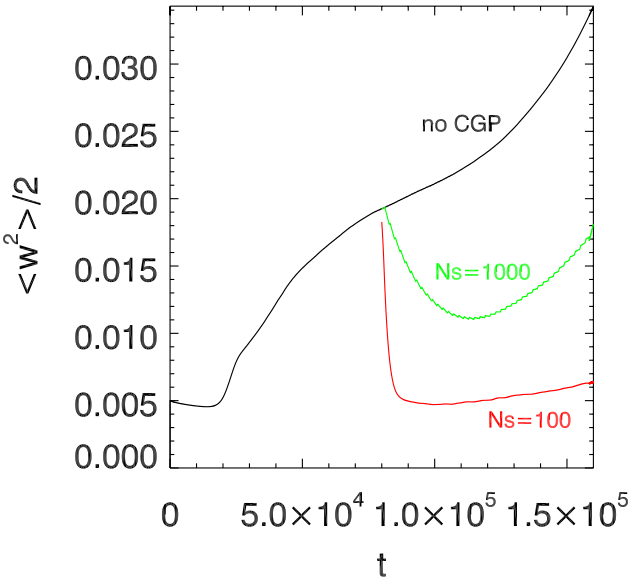

FIG. 2. (Color online) Coarse-graining effect on electron weight. Simulation started with no CGP until $\omega_{ci}t=8\times10^4$, then restarted for three identical runs with no CGP, CGP with $N_s=1000$, $\delta=0.1$, and CGP with $N_s=100$, $\delta=0.1$.

mental core plasmas. For all the δ values and e-i collisional rates, the simulated mode growth rate and frequency are essentially the same. In fact, this linear observation suggests that, for the purpose of studying anomalous ion heat transport, e-i collisional effects are not worth preserving. Here we use the results in Fig. 1 only in an attempt to quantify the effect of coarse graining and compare it with physical dissipation effects. Figure 1 shows that both CGP and e-i collisions drive the particle flux from negative values (particle pinching) at low dissipation to positive at high dissipation, but collisions are more effective. For given coarse-graining parameters (N_s, δ) one can define an equivalent collision rate to be that which yields the same Γ_p/Γ_{ei}. Thus for $\delta/N_s=0.001$, a typical value used in nonlinear simulations, the equivalent collision rate is effectively zero. At $\delta=0.5$ the dissipation due to CGP is 50 that of $\delta=0.01$; the CGP-driven particle flux is positive, but still below the "experimental" value.

In order to demonstrate that nonlinear effects of e-i collisions are also preserved by CGP, we use a plasma profile based on the Cyclone Base Case.[3] The temperature profile is given by

$$\frac{T(s)}{T(s_0)} = \exp\left(-\frac{a\Delta s}{L_0}\tanh\frac{s-s_0}{\Delta s}\right), \tag{4}$$

with $s=r/a$, $a=256.92\rho_i$, $L_0=100\rho_i$, and $s_0=0.5$. A similar analytic form is used for the density profile. Other parameters are $m_i/m_p=1$ (m_p is the proton mass), $R_{maj}=713.7\rho_i$, $r_0=128.46\rho_i$, $L_n/\rho_i=450$, $L_T/\rho_i=150$, $\Delta s=0.6$, $a/\rho_i=257$, $R_0/\rho_i=737$. The q-profile is given by

$$q(s) = 1 + 0.43s^2 + 2.33s^3, \tag{5}$$

with $q_0(r_0)=1.4$ and $\hat{s}_0=0.8$. The simulation domain is $(0.325a, 0.675a)$. Plasma beta is fixed, $\beta=0.012$. The e-i collision rate is $\nu_{ei}/\omega_{ci}=0.0001$. We first run the simulation without CGP for 40000 steps ($\omega_{ci}\Delta t=2$), then continue the simulation for 40000 steps with CGP for (a) $\delta=0$; (b) $N_s=100$, $\delta=0.1$; and (c) $N_s=1000$, $\delta=0.1$. The evolution of the mean square of the electron weights and the electron particle flux is plotted is Figs. 2 and 3. The electron flux is positive in all three simulations. The particle diffusivities, averaged for the time window $80000\omega_{ci}t$ to $160000\omega_{ci}t$, are $D_e/L_n v_{Ti}=0.116$, 0.122, and 0.120, respectively, for cases (a), (b), and (c). The electron weights, on the other hand, are effectively reduced in the cases with coarse-graining, as can be seen in Fig. 2. We note that the particle fluxes in all three simulations continue to decrease slowly in later times. This is likely due

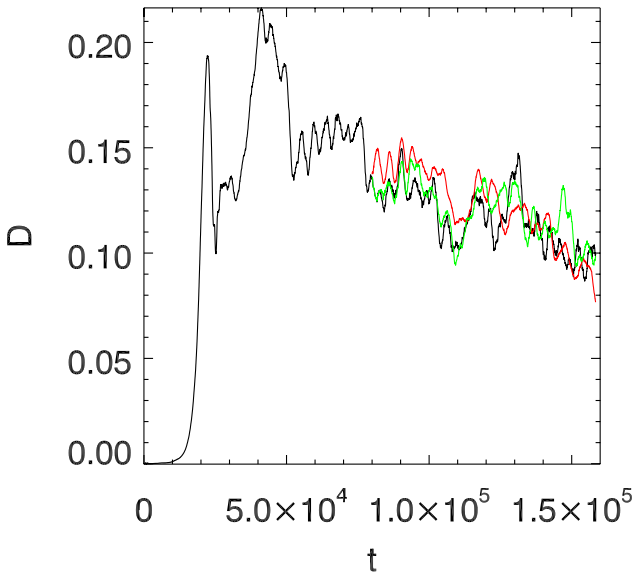

FIG. 3. (Color online) Normalized particle diffusivity $DL_n/\rho_i v_{Ti}^2$ vs time for the three cases in Fig. 2 (with matching color). Coarse-graining does not change the nonlinear particle flux.

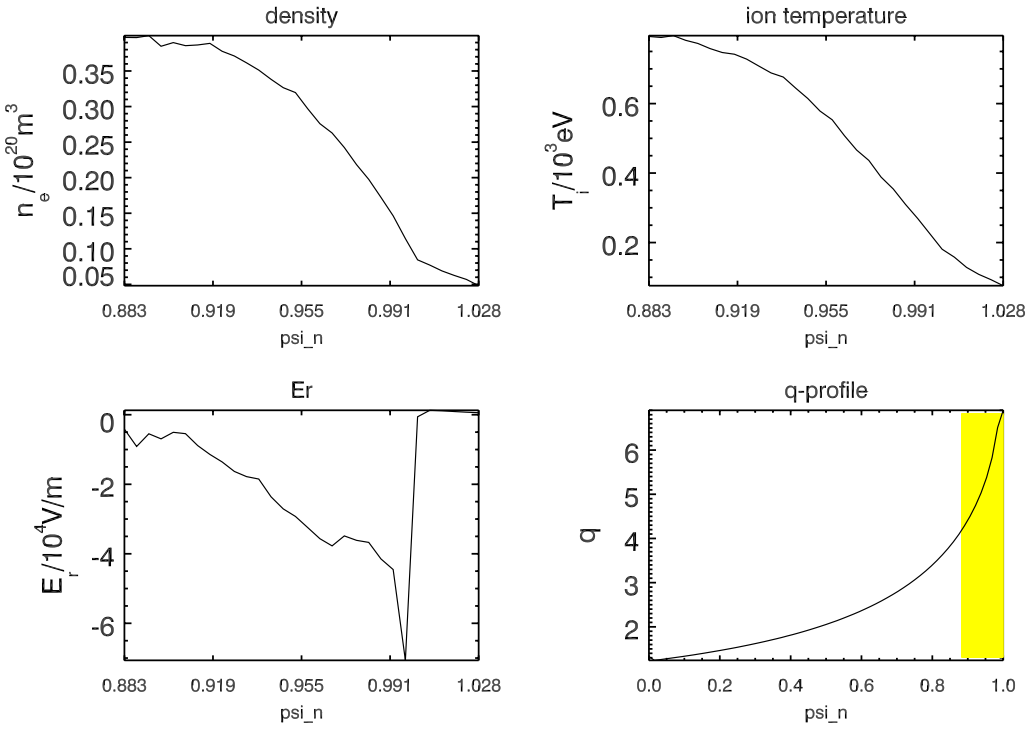

FIG. 4. (Color online) Density, ion temperature, E_r, and safety factor vs the normalized poloidal flux, from XGC simulations. The marked region in the q-profile is the simulation domain.

to slow profile relaxation caused by turbulent transport, since no attempt is made to prevent the density and temperature profiles from relaxing.

IV. EDGE PEDESTAL SIMULATION

In flux-tube simulations of TEM turbulence,[11] it is found that when the density gradient is large, $R/L_n > 10$, the instabilities grow to large amplitudes without saturating, eventually violating the gyrokinetic ordering for ion-Larmor-radius fluctuations, $e\phi/T \ll 1$. Since a density gradient of $R/L_n > 10$ is typical of edge plasmas, the stabilizing mechanism for such plasmas is of interest. Here we present an example of edge plasma simulation that illustrates the importance of equilibrium $\mathbf{E}\times\mathbf{B}$ flow and magnetic perturbation. Throughout this section, CGP is done with $N_s=100$ and $\delta=0.1$.

The plasma profiles used in the GEM simulation are output from an XGC0[10] simulation of a DIII-D plasma. XGC0 is an ion-electron-neutral guiding center particle code using a realistic numerical magnetic equilibrium and wall geometry from the EFIT code.[13] Due to non-Maxwellian ions, neutral ionization source, and the wall loss, the full-function (full-f) simulation technique is used. The numerical magnetic geometry includes the separatrix and the magnetic X-point. XGC0 has been developed out of the original ion-neutral XGC code.[14] XGC0 uses the Lagrangian guiding-center equation of motion of plasma ions and electrons, and Monte Carlo flights of the neutral atoms with a specified wall recycling coefficient. The Monte Carlo–Coulomb collisions conserve particle, momentum, and energy. Neutral atoms and the plasma species undergo charge exchange, ionization, and electric collisions. The radial electric field profile is solved for self-consistently with the plasma dynamics, which is an essential feature in this study. In order to model a turbulence diffusion onto the particle motion, an ambipolar radial random walk is superposed to the Lagrangian ion and electron motions. A more detailed description on the fundamental features of the XGC0 code can be found in the original XGC code introduction in Ref. 14. XGC0 can run either with or without electrons. We find that when we build up the pedestal by neutrals starting from a mild slope in an axisymmetric geometry, the neoclassical ion dynamics dominates the radial electric field solution and the plasma evolution. On the other hand, when a steep pedestal profile is relaxed by a lack of neutrals or when there is a nonaxisymmetric magnetic field component, inclusion of the electron dynamics is essential. In the pedestal buildup simulation results presented here in an axisymmetric geometry, we turned off the electron dynamics for a faster simulation time. The neutral wall recycling coefficient is assumed to be 0.999. An external momentum source (such as neutral beams) is assumed to be absent. A random-walk diffusion coefficient of 0.1 m^2/s is used to yield a better fit to the experimental edge plasma profile. In the near future, the particle and heat fluxes evaluated from the GEM code will be fed back into XGC0 for a more tightly coupled simulation between the two codes. Eventually, XGC0 will be replaced by the XGC1 gyrokinetic edge turbulence code for a self-contained neoclassical-turbulence edge simulation.

The q-profile, ion temperature, and density profiles and the radial electric field profile across the pedestal are shown in Fig. 4. The electron temperature is assumed to be $T_e = 0.75T_i$. The simulated radial slice is $0.91 < r/a < 0.99$. The

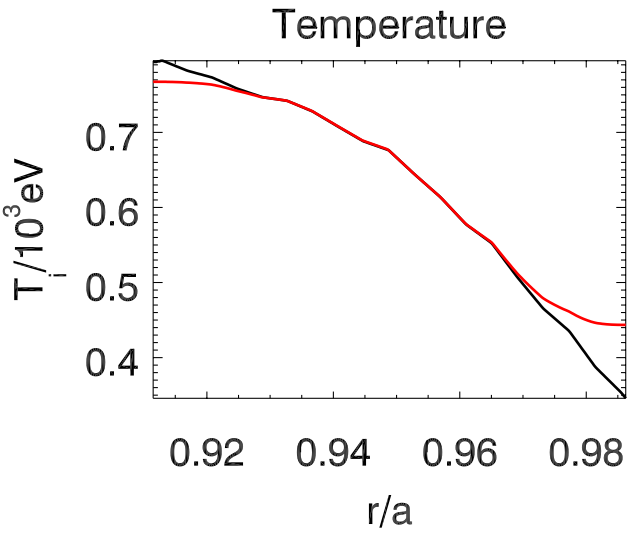

FIG. 5. (Color online) XGC temperature profile (black) and the modified profile for GEM simulation (red/light gray).

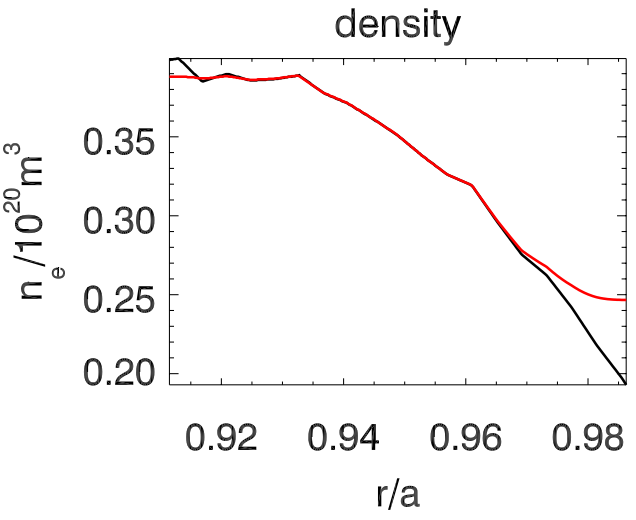

FIG. 6. (Color online) XGC electron density profile (black) and the modified profile (red/light gray).

surface shape parameters, elongation, and triangularity are taken to be constant in this radial slice, $\kappa=1.59$ and $\delta=0.128$. The safety factor is $q_0=5.3$ at $r/a=0.95$, with $\Delta q=1.9$ across the radial box. The q-profile is assumed to be linear. The width of the simulation domain is $L_x=24\rho_i$, with ρ_i the thermal deuterium Larmor radius calculated at the inner boundary. This radial domain size is quite small in terms of the thermal ion Larmor radius, as expected for a pedestal, in which a significant fraction of the ions have trajectories that cross the separatrix. In GEM simulations, fixed boundary conditions are assumed. The electric potential and the vector potential are assumed to be zero at the radial boundaries, and particles crossing the boundaries are relocated at the point following the unperturbed trajectories.[4] Thus one must bear in mind that the validity of the simulation is limited to a time scale much shorter than the ion transit time. This limitation is partly alleviated by the fact that for the case considered, within the instability growth time ($\sim 1/\gamma$), the number of ions crossing the boundaries is a small fraction of the total. Let ω_{ci} be the proton Larmor frequency (used for normalizing time in GEM). For $\gamma/\omega_{ci}=0.0003$, the fraction of ions crossing the boundaries in a growth time is numerically found to be less than 5%.

To avoid an instability drive that peaks near the boundaries, the ion temperature and density profiles are modified near the boundaries as shown in Figs. 5 and 6. The minimum of the density scale length occurs at $r/a\approx 0.96$ with $R/L_n\approx 50$.

The turbulent transport coefficients are obtained as follows. First a volume averaged turbulent heat flux Γ_i is computed. Then a temperature gradient defined as $\nabla T=\Delta T/\Delta r$, with ΔT the temperature change over the simulation width Δr, is used to convert the heat flux into a heat diffusivity χ_i,

$$\Gamma_i = n_{96}\chi_i \frac{\Delta T_i}{\Delta r}, \tag{6}$$

where n_{96} is the ion density at $r/a=0.96$. The electron heat diffusivity is similarly calculated. The particle flux Γ_p is converted into the particle diffusivity D according to

$$\Gamma_p = D\frac{\Delta n}{\Delta r}, \tag{7}$$

where Δn is the change of density across Δr.

We first carry out electrostatic simulations. This is done by setting $\beta_i=\mu_0 n_0 T_{i0}/B^2=7\times 10^{-5}$ from its original value of 0.00143 (here n_0 and T_{i0} are density and ion temperature at the inner boundary). Such a small β_i is not expected to be important, but allows a relatively larger time step compared with $\beta_i=0$. This is equivalent to reducing the plasma density to 1/20 of the original value. To study the dependence of transport on the $\mathbf{E}\times\mathbf{B}$ flow level, we multiply the E_r profile by a scaling factor, and observe the change in the transport coefficients. The results are shown in Fig. 7. The electron heat diffusivities for three runs with scaling factors of 0.75, 1.0, and 1.25 are shown in Fig. 8. The average transport coefficients over the time window $60000<\omega_{ci}t<90000$ are used in Fig. 7. The ion heat diffusivity decreases from 0.21 m^2/s at the original flow level to 0.06 m^2/s at 1.25 times the original level.

The corresponding results for the original beta value $\beta_i=0.00143$ are shown in Fig. 9. The plasma is more unstable. The ion heat diffusivity increases from $\chi_i=0.21$ m^2/s in the electrostatic case to $\chi_i=3.4$ m^2/s in the electromagnetic case. In fact, the instabilities are so strong as to cause significant relaxation of the ion pressure profile, as shown in Fig. 10. This calls into question the interpretation of the results of gyrokinetic simulation when significant profile relaxation occurs. One can either allow the profiles to freely relax and account for the relaxation effect by interpreting the results as a time-dependent transport coefficient in a relaxing profile, or adopt additional numerical procedures to prevent the profile from relaxing. It must be noted that in GEM simulations, the marker particles are loaded in velocity according to the assumed equilibrium distributions. The perturbed pressure profile in Fig. 10 is obtained by adding the perturbed pressure δP, obtained from δf_i, to the initial pressure profile. As

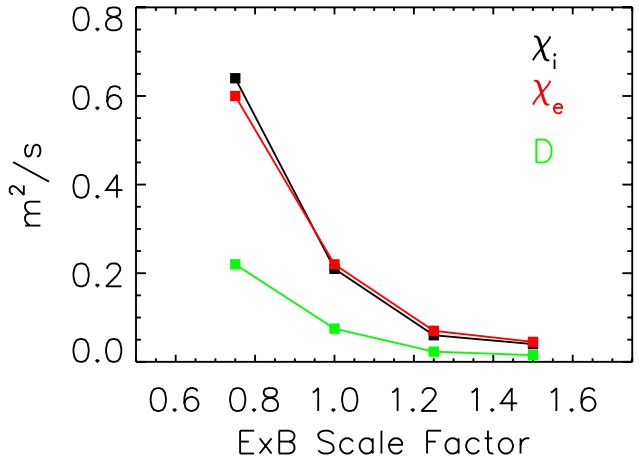

FIG. 7. (Color online) Volume averaged transport coefficients vs $\mathbf{E}\times\mathbf{B}$, electrostatic.

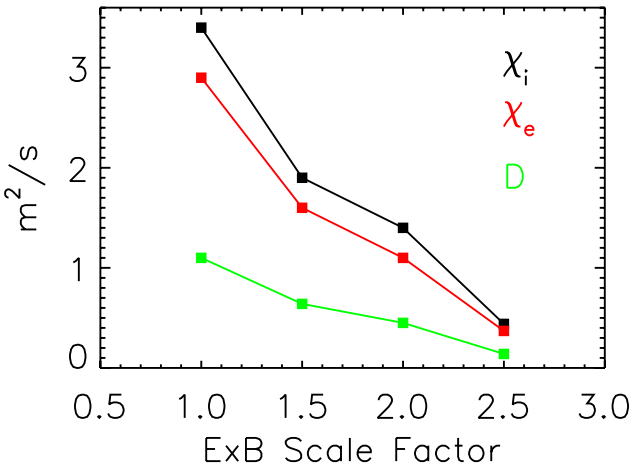

FIG. 9. (Color online) Volume averaged transport coefficients vs $\mathbf{E}\times\mathbf{B}$, electromagnetic.

δP grows in the simulation, the marker particle distribution will also change accordingly. Thus the issue of preventing profile relaxation in PIC simulations is always twofold: one not only needs to add an appropriate source term in the weight evolution equation (as, for instance, in global ITG simulation[15]), but also needs to ensure that the marker distribution is close to the assumed form, perhaps through introducing particle sources and sinks into the simulation. This is particularly important for simulating pedestal plasmas on the neoclassical time scale. We plan to address this problem in the future.

Since the local plasma beta is much lower than typical core values, the enhancement of instability growth rates and transport levels is due to the strong density and temperature gradients. We have carried out simulations with a flattened ion temperature profile, electron temperature profile, and density profile, respectively. Flattening the ion temperature profile results in little change in the instability growth rates, whereas flattening the density profile causes the largest reduction. Thus the dominant instabilities appear to be driven by the electrons. This conclusion is confirmed by an examination of the unstable mode spectrum. The linear growth rates of different toroidal modes are shown in Fig. 11 for both electrostatic and electromagnetic cases. The growth rate increases with n for $n>20$ in the electrostatic case. This is consistent with previous linear results from flux-tube simulations.[11] The fact that γ increases with n for these high-n modes and that finite-β has a stabilizing effect on them suggests that they are electron drift waves. Near $n=10$ there is a peak in the growth rates, and these modes are further destabilized by finite-β effects. Since magnetic perturbation is mainly generated by perturbed electron current, the enhancement to turbulent transport due to finite-β effects es-

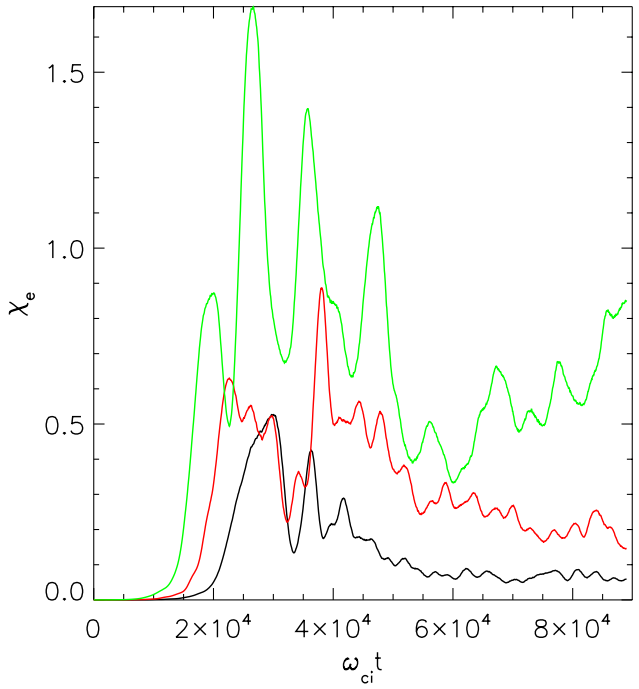

FIG. 8. (Color online) Electron heat diffusivity vs time for the three cases in Fig. 7 with $\mathbf{E}\times\mathbf{B}$ scaling factor of 0.75 (green/gray), 1.0 (red/light gray), and 1.25 (black), respectively.

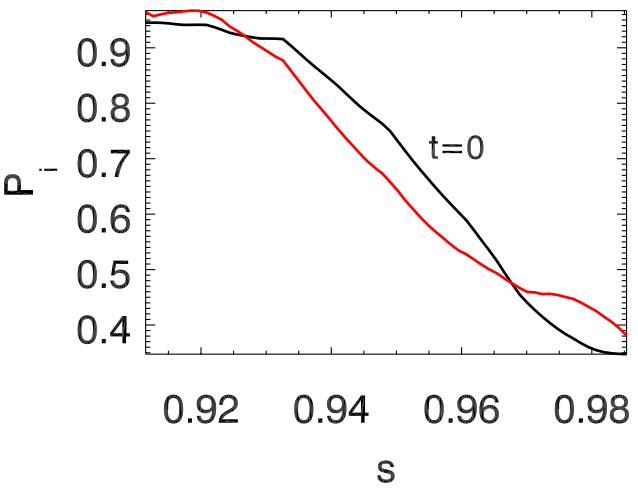

FIG. 10. (Color online) Ion pressure profile at the beginning (black) and end (red) of the electromagnetic run with $\mathbf{E}\times\mathbf{B}$ scaling factor of 1.0.

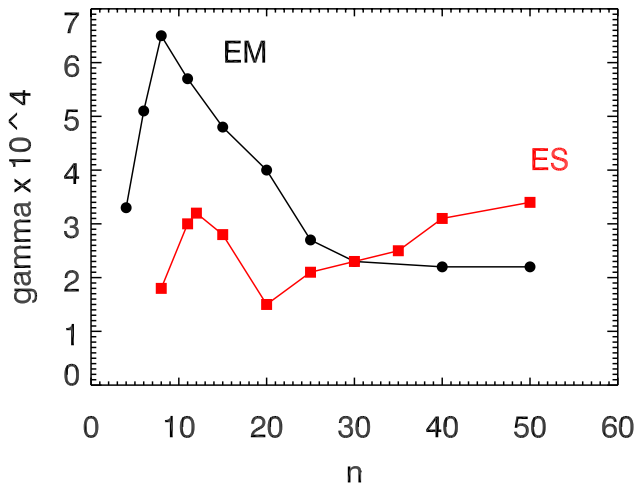

FIG. 11. (Color online) Mode growth rate vs toroidal mode number, with (EM) and without (ES) magnetic field perturbations.

sentially comes from the electron response to the magnetic perturbations. However, the enhanced growth rates around $n=10$ are not due to the destabilization of a different branch of modes such as the kinetic ballooning modes (KBM) that become unstable at large β in core plasmas. As shown in Fig. 12, as the growth rate of the $n=11$ mode continuously increases with β, the mode real frequency, while slowly decreasing, does not display a jump as would be expected from a transition to KBM.

V. CORE SIMULATION

As an example of application of the GEM code to a realistic core plasma case, profiles from a DIII-D[16] discharge with moderate ion temperatures and moderate toroidal rotation speeds are employed. The density and temperature profiles for each of the four plasma species, background deuterium, carbon impurity, hot beam deuterium, and electrons, along with the radial profiles of the parallel flow velocities for each of the ion species, are obtained from the TRANSP system. A radial profile of the equilibrium electrostatic potential is calculated by the NCLASS code from radial force

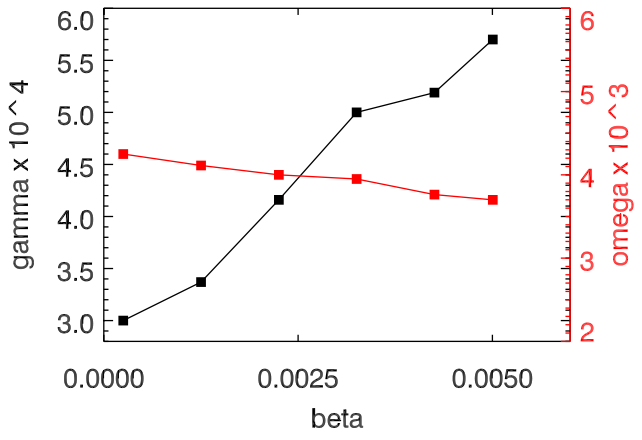

FIG. 12. (Color online) Mode growth rate and frequency for $n=11$ vs beta.

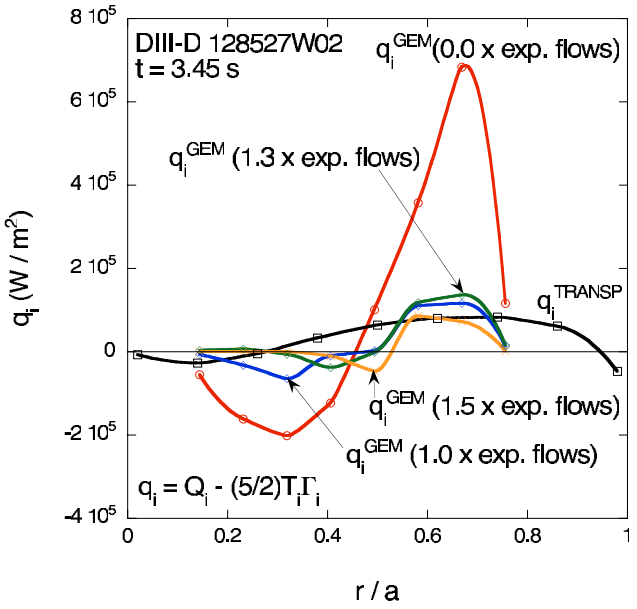

FIG. 13. (Color online) Ion heat flux profiles in DIII-D core plasma simulations with different $\mathbf{E}\times\mathbf{B}$ scaling factors.

balance, and this is used by the GEM code to calculate the $\mathbf{E}\times\mathbf{B}$ velocity profile. In addition, profiles of total pressure and of (surface-averaged) parallel current, along with the plasma boundary shape, from the TRANSP system are used as input for a high-resolution run of the JSOLVER MHD equilibrium code, which among other things calculates the resulting radial profiles of ellipticity, triangularity, major radius, and q. These profiles in turn are the input for the Miller MHD equilibrium implemented in the GEM code. Then a global nonlinear GEM code run including trapped electrons, electron collisions, electromagnetic effects (Φ and $A_\parallel$), and the three ion species, employing the CGP, is carried out, with the input $\mathbf{E}\times\mathbf{B}$ velocity profile and the parallel velocity profiles multiplied by a constant, C. When $C=0$ (no flows), the computed thermal (background deuterium plus carbon) heat fluxes q_i, time-averaged over the end of the nonlinearly saturated period, are much larger than the experimental heat fluxes from the TRANSP system. However, for $C=1.0$, the radial-maximum heat flux is only moderately larger than that from TRANSP, and for $C=1.5$ they are essentially the same, as is shown here in Fig. 13. On the other hand, the width of the q_i peak from TRANSP is much broader than that from the GEM calculation, since TRANSP does a considerable amount of radial smoothing. For $C\leq 1.0$, and with some amount of additional radial smoothing of the results from GEM, it would be possible to match the TRANSP q_i profile reasonably well. These results are preliminary, but serve to show the results of which the GEM code is capable.

VI. SUMMARY

The coarse-graining procedure has been implemented in the GEM code. The quasilinear particle pinch of ITG instabilities is used to study the effect of numerical dissipation arising from CGP, and compare it with the effect of electron-ion collisions. It is found that for typical CGP parameters,

the numerical dissipation of CGP is very small. Nonlinear convergence studies show that CGP also preserves collisional effects on the particle diffusivity. An example of simulation of plasmas with strong density and temperature gradients is presented. The essential role of the shear $\mathbf{E}\times\mathbf{B}$ flow in stabilizing such plasmas is demonstrated. An interesting observation of such a plasma is that the drift wave instabilities are enhanced by finite-β effects, without apparent transition to a different branch of instabilities. An example of applying GEM to DIII-D core plasmas is also presented.

[1]Y. Chen and S. E. Parker, Phys. Plasmas **14**, 082301 (2007).
[2]K. Hallatschek and W. Dorland, Phys. Rev. Lett. **95**, 055002 (2005).
[3]A. Dimits, G. Bateman, M. A. Beer *et al.*, Phys. Plasmas **7**, 969 (2000).
[4]Y. Chen and S. E. Parker, J. Comput. Phys. **220**, 839 (2007).
[5]R. L. Miller, M. S. Chu, J. M. Greene, Y. R. Lin-Liu, and R. E. Waltz, Phys. Plasmas **5**, 973 (1998).
[6]R. Waltz and R. L. Miller, Phys. Plasmas **6**, 4265 (1999).
[7]R. Goldston, *Basic Physical Processes of Toroidal Fusion Plasmas*, Proc. Course and Workshop, Varenna (Monotypia Franchi, Città di Castello, 1985), Vol. 1, p. 165.
[8]W. A. Houlberg, K. C. Shaing, S. P. Hirshman, and M. C. Zarnstorff, Phys. Plasmas **4**, 3231 (1997).
[9]J. DeLucia, S. C. Jardin, and A. M. M. Todd, J. Comput. Phys. **37**, 183 (1980).
[10]G. Park, J. Cummings, C. S. Chang, N. Podhorszki, S. Klaski *et al.*, J. Phys.: Conf. Ser. **78**, 012087 (2007).
[11]J. Lang, Y. Chen, and S. E. Parker, Phys. Plasmas **14**, 082315 (2007).
[12]Y. Chen and S. E. Parker, J. Comput. Phys. **189**, 463 (2003).
[13]L. L. Lao, H. S. John, R. D. Stambaugh, A. G. Kellman, and W. Pfeiffer, Nucl. Fusion **25**, 1611 (1985).
[14]C. S. Chang and S. Ku, Phys. Plasmas **11**, 5626 (2004).
[15]Z. Lin, S. Ethier, T. S. Hahm, and W. M. Tang, Phys. Rev. Lett. **88**, 195004 (2002).
[16]J. L. Luxon, Fusion Sci. Technol. **48**, 828 (2005).